# From Isolated Complex Units to One-Dimensional Molecular Chains: Optical Investigations of Ternary Alkali-Metal Thioferrates(III)

**Rolf Packroff and Hans-Herbert Schmidtke***

Institut für Theoretische Chemie, Heinrich-Heine-Universität, D-4000 Düsseldorf 1, Germany

*Received February 27, 1992*

Low-temperature absorption spectra in the near-infrared and visible region were recorded from KBr disks of iron–sulfur complexes which contain (pseudo-) tetrahedral [$Fe^{III}S_4$] units in their crystal structures, i.e., $Na_5FeS_4$, with isolated tetrathioferrate(III) chromophores, dimer $Na_3FeS_3$ and the chain compounds $AFeS_2$ (A = K, Rb, Cs). Also, polarized measurements were carried out on $CsGa_{1-x}Fe_xS_2$ ($0.00 \le x \le 0.25$) mixed crystals. The spectra are dominated by intense bands in the visible region which are assigned to LMCT transitions of the [$Fe^{III}S_4$] chromophore. The lowest CT transition measured from the mixed crystals is strongly $z$-polarized ($\vec{E} \parallel$ chain axis) and exhibits band-edge behavior even at low iron concentrations. With increasing iron content the band-edge is shifted to lower energies, indicating formation of higher oligomers. Several weak transitions measured at higher sensitivity between 8000 and 17 000 $cm^{-1}$ are assigned to the d–d transitions of a high-spin $d^5$ chromophore using polarization selection rules. On this basis also shoulders and inflections measured from the pure ferric compounds can be interpreted by comparison. A fit of band peaks by angular-overlap calculations leads to ligand field parameters smaller than those of the $[FeCl_4]^-$ analogue. From CT transitions an optical electronegativity of 2.5 for the sulfur ligand is derived. The strong antiferromagnetic coupling between the iron units in polycenter complexes affects primarily band intensities and the energies of CT transitions. A low-spin ground state, which was assumed on the basis of magnetic measurements on some of these systems, could not be confirmed from present optical investigations.

## Introduction

Electronic, magnetic, and optical properties of compounds containing tetrahedral $FeS_4$ units in their crystal structures are of considerable interest for an understanding of electron transport mechanisms in analogous iron–sulfur proteins.[1,2] Ternary alkali-metal thioferrates(III) synthesized in recent years[3-5] provide good model compounds for these investigations. $Na_5FeS_4$ is the only known ternary compound with isolated $[FeS_4]^{5-}$ tetrahedra which are slightly distorted,[6] and $Na_3FeS_3$ has two edge-sharing tetrathioferrate(III) units in the solid state.[7] Linear chains of $[FeS_2]^-$ units with an approximate $D_{2d}$ site symmetry (stretched along the $S_4$ axis) are present in $AFeS_2$ (A = K, Rb, Cs).[8,9] $CsGaS_2$ belonging to the same structure as $KFeS_2$ and $RbFeS_2$ can be used as host material, substituting about 25% of Ga for Fe without change of crystal structure.[10]

Magnetic measurements at temperatures higher than the Néel point at 28 K show Curie–Weiss behavior for $Na_5FeS_4$ with an effective magnetic moment of 5.6 $\mu_B$ (the five unpaired electrons spin-only value is 5.92 $\mu_B$)[6] and low susceptibilities of $Na_3FeS_3$, indicate strong antiferromagnetic coupling between the iron centers.[11] The magnetic moments of $AFeS_2$ compounds, which are semiconductors along the $[FeS_2]$ chain,[12] do not depend very much on temperature.[3,9,13-15] Neutron diffraction studies on $KFeS_2$ and $RbFeS_2$ yield effective magnetic moments of, respectively, 2.6 and 2.7 $\mu_B$ on the iron site, and Mössbauer spectra show low hyperfine fields compared to those of other Fe(III) complexes.[11,15] Extensive grinding of $CsFeS_2$ leads to products which show Curie–Weiss behavior with $\mu_{eff}$ = 1.7 $\mu_B$/Fe.[10] On the basis of these observations a low-spin ground state of $S = {}^1/_2$ for iron has been assumed for the chain compounds,[3,11,15] which is unusual for tetrahedral coordination for a weak field ligand like sulfur. Mixed crystals of $CsGa_{1-x}Fe_xS_2$ approximately obey the Curie–Weiss law with $\mu_{eff}$ = 5.39 $\mu_B$ for small concentration ($x$ = 0.01) and 2.66 $\mu_B$ for $x$ = 0.20.[10]

Optical properties have been reported earlier for the chain compounds $AFeS_2$ and $CsGa_{1-x}Fe_xS_2$ in KBr and TlCl disks or in silicone grease.[16-18] The absorption spectra of the pure ferric compounds are dominated by three broad maxima at about 15 100, 18 800, and 23 000 $cm^{-1}$, which have been assigned to d–d transitions of a high-spin $d^5$ chromophore.[17] Later the same bands were interpreted as ligand-to-metal charge transfer transitions (LMCT) on the basis of a spin-polarized multiple scattering $X\alpha$ calculation performed on a $[FeS_4]^{5-}$ unit.[19] Ligand field (LF) calculations may support, however, an assignment to d–d transitions in a low-spin $d^5$ system, in accordance with magnetic and Mössbauer measurements.[18]

One main reason for the assignment problem regarding the compounds with extended structures is the lack of information on isolated [$Fe^{III}S_4$], which can be used as a starting point for the discussion. In this connection, some results supplied by polarized single crystal absorption and MCD spectra of a $[Fe(SR)_4]^-$ anion (R = 2,3,5,6-$(Me)_4C_6H$)[20,21] are of interest. Between 7250 and 11 225 $cm^{-1}$ they exhibit the lowest d–d

* To whom correspondence should be addressed.

(1) Lovenberg, W. *Iron-Sulfur-Proteins*; Academic Press: New York: 1973, Vols. I and II; 1977, Vol. III.
(2) Spiro, T. G. *Metal Ions in Biology. Iron Sulfur Proteins*; Wiley-Interscience: New York, 1982.
(3) Bronger, W. *Angew. Chem.* **1981**, *93*, 12.
(4) Bronger, W.; Müller, P. *J. Less-Common Met.* **1984**, *100*, 241.
(5) Bronger, W. *Pure Appl. Chem.* **1985**, *57*, 1363.
(6) Klepp, K. O.; Bronger, W. *Z. Anorg. Allg. Chem.* **1986**, *532*, 23.
(7) Müller, P.; Bronger, W. *Z. Naturforsch.* **1979**, *34B*, 1264.
(8) Boon, J. W.; MacGillavry, C. H. *Recl. Trav. Chim. Pays-Bas* **1942**, *61*, 910.
(9) Bronger, W. *Z. Anorg. Allg. Chem.* **1968**, *359*, 225.
(10) Bronger, W.; Müller, P. *J. Less-Common Met.* **1980**, *70*, 253.
(11) Müller, P. Thesis, Universität Aachen, 1980.
(12) Cowan, D. O.; Pasternak, G.; Kaufman, F. *Proc. Natl. Acad. Sci. U.S.A.* **1970**, *66*, 837.
(13) Johnston, D. C.; Mraw, S. C.; Jacobson, A. J. *Solid State Commun.* **1982**, *44*, 255.
(14) Mauger, A.; Escorne, M.; Taft, C. A.; Furtado, N. C.; Arguello, Z. P.; Arsenio, T. P. *Phys. Rev.* **1984**, *B30*, 5300.
(15) Bronger, W.; Kyas, A.; Müller, P. *J. Solid State Chem.* **1987**, *70*, 262.
(16) Rawlings, J.; Siiman, O.; Gray, H. B. *Proc. Natl. Acad. Sci. U.S.A.* **1974**, *71*, 125.
(17) Taft, C. A.; de Paoli, M. A. *Chem. Phys. Lett.* **1979**, *68*, 94.
(18) Schmidtke, H.-H.; Packroff, R.; Bronger, W.; Müller, P. *Chem. Phys. Lett.* **1988**, *150*, 129.
(19) Taft, C. A.; Braga, M. *Phys. Rev.* **1980**, *B21*, 5802.
(20) Deaton, J. C.; Gebhard, M. S.; Koch, S. A.; Millar, M.; Solomon, E. I. *J. Am. Chem. Soc.* **1988**, *110*, 6241.

0020-1669/93/1332-0654$04.00/0 

transitions of a high-spin $d^5$ chromophore of compressed $S_4$ symmetry in accordance with ab-initio calculations predicting the lowest spin-forbidden LF excitation for isolated species at about 8000 $cm^{-1}$.[22,23] CT transitions of this complex appear above 13 000 $cm^{-1}$ with intensities of $\epsilon > 300$ L $mol^{-1}$ $cm^{-1}$.[21] More recently it has been shown that photoelectron results on $KFeS_2$ obtained from variable input radiative energy are conveniently explained by spin orbital diagrams calculated from unrestricted $X\alpha$ calculations on $FeS_4^{5-}$.[24]

The present work offers first of all an assignment of S → Fe charge-transfer bands in the spectrum of $Na_5FeS_4$ using the results on the $FeCl_4^-$ analogue.[25] Subsequently the implications of strong antiferromagnetic coupling on these transitions is discussed as measured for $Na_3FeS_3$ and $CsGa_{1-x}Fe_xS_2$ mixed crystals. From the latter compounds single crystals were available which are large enough for recording polarized spectra. Polarizations due to low symmetry effects are interpreted on the basis of symmetry selection rules and by extended-Hückel (EHMO)[26] and angular overlap model (AOM)[27] calculations. Trends observed with increasing iron content of $CsGa_{1-x}Fe_xS_2$ lead to new assignments of band maxima of the pure $AFeS_2$ chain compounds.

The assignment of d–d transitions in the polarized spectra of $CsGa_{1-x}Fe_xS_2$ is carried out using the same models. AOM calculations offer the advantage of furnishing results which depend only on two parameters when chromophores with identical ligands and low symmetry are considered.[28] Comparison of $Na_5FeS_4$, $Na_3FeS_3$, and $AFeS_2$ spectra is useful for discussing antiferromagnetic coupling and possible spin changes when going from isolated $[FeS_4]$ to $[FeS_2]$ chains.

A main object of interest is a closer characterization of the sulfur ligand in transition metal complexes, (previous investigations deal with metal ions doped in sulfuric hosts, e.g., ZnS or CdS[29-31]): a classification into the spectrochemical and nephelauxetic series[32] and an estimation of the optical electronegativity[31,33] would be most helpful. The effect of antiferromagnetic coupling on CT and d–d transitions of the cluster and chain compounds can be discussed in view of EHMO calculations on the $[FeS_2]$ chain by Silvestre and Hoffmann.[34] Comparison is also made with corresponding optical properties of weak antiferromagnets.[35]

## Experimental Methods

**Absorption Measurements. $Na_5FeS_4$, $Na_3FeS_3$, $CsGa_{1-x}Fe_xS_2$, and $AFeS_2$** compounds have been supplied by Bronger and Müller.[6,7,9,10] For absorption measurements a small amount of powders was ground with an excess (20–50 times) of carefully dried KBr in a glovebox under an argon atmosphere and pressed to generally transparent pills (thickness ~2 mm). Also inside the box the disks were mounted on the sample holder of an Air Products LT-3-110C helium cryostat by a deep-temperature glue (GE 7031, Cryophysics GmbH). Absorption spectra were taken on a Varian Cary 17 spectrophotometer equipped with a special focusing device necessary for integrating the helium cryostat into the light path.[36] Cooling of the sample down to about 15 K was reached. For detection in the range between 11 200 and 40 000 $cm^{-1}$ an RCA 4832 photomultiplier was used, near-IR signals were detected by a PbS photo cell (4500–11 500 $cm^{-1}$).

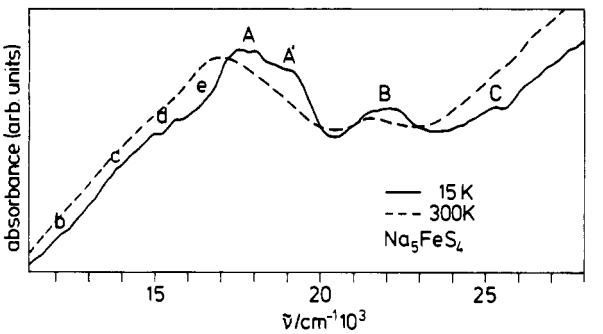


**Figure 1.** Absorption spectrum of $Na_5FeS_4$ measured from a KBr disk at room temperature and at 15 K.

The technique used for investigating KBr disks with high iron compound concentrations (necessary for detecting low-intensity bands) was different (equipment for scattering samples = ESS). To avoid loss of scattered light, the pellet was mounted directly on the surface of a germanium diode (APYIII, Siemens) which was placed into the sample holder of a closed-cycle cryostat (Air Products CSA-202). When the KBr disks were handled outside the glovebox, they were protected from moisture by a skin formed by a suitable spray (Letraspray Schutzlack G, Letraset GmbH). The broad absorption band of this spray near 7000 $cm^{-1}$ does not interfere with the absorptions in the near-IR/vis region of the components.[37] The equipment contained a tungsten lamp (100 W, Osram), a chopper, a 0.75m-Spex monochromator, an edge-filter for reducing higher order inflections, a lock-in-amplifier (Dynatrac 391A, Ithaco), the detector system described above, and a recorder. This allows measurements between 7400 and 20 000 $cm^{-1}$ at a temperature of about 20 K. For subtraction of the background the spectra were digitized and processed on a microcomputer.

**$CsGa_{1-x}Fe_xS_2$** was available as transparent crystals (minimum 1 mm × 1 mm). The Fe content indicated is calculated from the mole ratios of educts applied in the synthesis. The polarized spectra were recorded from samples using an aluminum carrier mounted on the sample holder of the cryostat. Polarization was obtained from a Glan-Taylor prism added into the light path of the Cary 17 spectrometer.[36] Absorption measurements on highly doped crystals displaying a metallic surface were possible by using the arrangement as described for ESS.

**Computational Details.** Extended-Hückel calculations were carried out with the programs FORTICON8[38] and EHMACC[39] supplied by QCPE which were modified for usage under BS2000 on the Siemens 7580-S computer at Düsseldorf University. The parameters of Silvestre and Hoffmann[34] were adopted. For AOM calculations an extended version of a FORTRAN77 program written by Hoggard[40] was used.

## Experimental Results and Assignments

**Charge-Transfer Transitions. $Na_5FeS_4$.** In Figure 1 the absorption spectrum taken from a KBr disk is illustrated. Apart from the broad maxima A and B, a fine structure arises at 15 K as well as shoulders between 12 000 and 16 000 and at 25 300 $cm^{-1}$. Also an absorption band D is identified at about 29 000 $cm^{-1}$ superimposed on the strongly increasing background of the scattering sample.

In Table I the lowest LMCT transitions for a tetrahedron with a high-spin metal ion $d^5$ configuration are presented. Since only one spin- and symmetry-allowed excitation ($^6A_1 \rightarrow {}^6T_2$) is possible

(21) Gebhard, M. S.; Deaton, J. C.; Koch, S. A.; Millar, M.; Solomon, E. I. *J. Am. Chem. Soc.* **1990**, *112*, 2217.
(22) Bair, R. A.; Goddard, W. A., III. *J. Am. Chem. Soc.* **1977**, *99*, 3505.
(23) Bair, R. A.; Goddard, W. A., III. *J. Am. Chem. Soc.* **1978**, *100*, 5669.
(24) Butcher, K. D.; Gebhard, M. S.; Solomon, E. I. *Inorg. Chem.* **1990**, *29*, 2067.
(25) Deaton, J. C.; Gebhard, M. S.; Solomon, E. I. *Inorg. Chem.* **1989**, *28*, 877.
(26) Hoffmann, R. *J. Chem. Phys.* **1963**, *39*, 1397.
(27) Schmidtke, H.-H. *Quantenchemie*; VCH Verlagsgesellschaft: Weinheim, Germany, 1987.
(28) Horrocks, W. DeW.; Burlone, D. A. *J. Am. Chem. Soc.* **1976**, *98*, 6512.
(29) Pappalardo, R.; Dietz, R. E. *Phys. Rev.* **1961**, *123*, 1188.
(30) Weakliem, H. A. *J. Chem. Phys.* **1962**, *36*, 2117.
(31) Lever, A. B. P. *Inorganic Electronic Spectroscopy, Studies in Physical and Theoretical Chemistry 33*, 2nd ed.; Elsevier: Amsterdam, 1984.
(32) Schläfer, H. L.; Gliemann, G. *Einführung in die Ligandenfeldtheorie*; Akademische Verlagsgesellschaft: Frankfurt/Main, 1967.
(33) Jørgensen, C. K. *Prog. Inorg. Chem.* **1970**, *12*, 101.
(34) Silvestre, J.; Hoffmann, R. *Inorg. Chem.* **1985**, *24*, 4108.
(35) McCarthy, P. J.; Güdel, H. U. *Coord. Chem. Rev.* **1988**, *88*, 69.
(36) Teutsch, U.; Schmidtke, H.-H. *J. Chem. Phys.* **1986**, *84*, 6034.
(37) Packroff, R. Thesis, Universität Düsseldorf, 1991.
(38) FORTICON 8, written by: Hoffmann, R.; et al. *QCPE Bull.* **1977**, *11*, 344; adapted for BS 2000 by K. Eifert, Universität Düsseldorf.
(39) EHMACC, written by: Whangbo, M.-H.; Evain, M.; Hughbanks, T.; Kertesz, M.; Wijeyesekera, S.; Wilker, C.; Zheng, C.; Hoffmann, R. *QCPE Bull.* **1989**, *9*, 61; adapted for BS 2000 by K. Eifert, Universität Düsseldorf.
(40) AOMX, written by: Hoggard, P. E.; North Dakota State University, Dept. of Chemistry. Extended version for use under BS 2000 with automatic fitting of parameters to experimental data (NAG routine E04FDF) by: Eifert, K.; Adamsky, H., Universität Düsseldorf.

**Table I.** Lowest LMCT Transitions of a Cubic High-Spin $d^5$ Chromophore Possible by Symmetry from the $^6A_1$ Ground State

| orbital transition | | excited level[a] | |
|---|---|---|---|
| | | symmetry-allowed | symmetry-forbidden |
| $1t_1 \rightarrow 2e$ | $n \rightarrow \pi^*$ | $^6T_2$ | $^6T_1$ |
| $1t_1 \rightarrow 4t_2$ | $n \rightarrow \pi^*, \sigma^*$ | $^6T_2$ | $^6A_2, ^6E, ^6T_1$ |
| $3t_2 \rightarrow 2e$ | $\pi, \sigma \rightarrow \pi^*$ | $^6T_2$ | $^6T_1$ |
| $3t_2 \rightarrow 4t_2$ | $\pi, \sigma \rightarrow \pi^*, \sigma^*$ | $^6T_2$ | $^6A_2, ^6E, ^6T_1$ |

[a] Sextet levels only.

**Table II.** Assignment of CT Bands in the Absorption Spectrum of $Na_5FeS_4$

| energy,[b] $cm^{-1}$ | center of gravity, $cm^{-1}$ | orbital transition | excited level | peak |
|---|---|---|---|---|
| <17 000 | | $2e \rightarrow 4t_2$ | d–d | |
| 17 500 | 18 000 | $1t_1 \rightarrow 2e$ | $^6T_2$ | A |
| 18 000 | | | | |
| 18 600 sh | | | | |
| 19 100 sh | | | d–d? | A′ |
| 21 400 sh | 21 900 | $1t_1 \rightarrow 4t_2$ | $^6T_2$ | B |
| 22 200 | | | | |
| 25 300 sh | | $3t_2 \rightarrow 2e$ | $^6T_2$ | C |
| (29 000)[a] | | $3t_2 \rightarrow 4t_2$ | $^6T_2$ | D |

[a] From UV measurement, uncertain. [b] Key: sh, shoulder.

per orbital, the spectrum of the pseudotetrahedral ion shows only four CT bands,[24,25] which have been assigned on the basis of MCD measurements to orbital transitions from ligand MOs $1t_1$ and $3t_2$ to 2e and $4t_2$.[41] Absorption spectra of complexes with isolated $[Fe^{III}S_4]$ chromophores like $[Fe(S_2\text{-}o\text{-xylyl})_2]^-$,[42-45] $[Fe(SR)_4]^-$ (R = 2,3,5,6-(Me)$_4$C$_6$H),[20,21,46] $[Fe(cys\text{-}R)_4]^-$,[47,48] and ferric rubredoxin,[1,2,49-52] which exhibit intense broad absorptions between 17 000 and 30 000 $cm^{-1}$, are more complex due to the large ligand systems in these compounds.

As for $[FeCl_4]^-$, the asymmetric band A of $Na_5FeS_4$ is assigned to the lowest CT transition ($1t_1 \rightarrow 2e$) (Table II). The shoulders to lower energy arise from d–d transitions (see below). Bands B and C correspond to a higher CT transition ($3t_2 \rightarrow 2e$), C being similarly weak as in the chloro complex spectrum. All features are shifted about 10 000 $cm^{-1}$ to lower energy compared to the chloro compound. Other than for $[FeCl_4]^-$, the lowest band A shows fine structure at low temperature. Ligand field calculations supply some reasons for assigning A′ to a d–d transition (see below) while the other structure of A may be due to deviations from cubic symmetry, to spin–orbit coupling or vibronic sidebands.

Differences between A and B as well as C and D LMCT transitions should correspond to $10Dq = E(t_2) - E(e)$.[31] They are 3900 and about 3700 $cm^{-1}$ (centers of gravity), i.e. smaller compared to the corresponding differences for $[FeCl_4]^-$ (4040 and 4450 $cm^{-1}$) in contrast to the usual spectrochemical series of ligands.[32] The $Dq$ value of 585 $cm^{-1}$ (absolute) derived from fitting d–d transitions (see below) is much higher, which can be explained by the reduced charge at the metal after LMCT excitation observed to lead generally to lower $Dq$ values.[31]

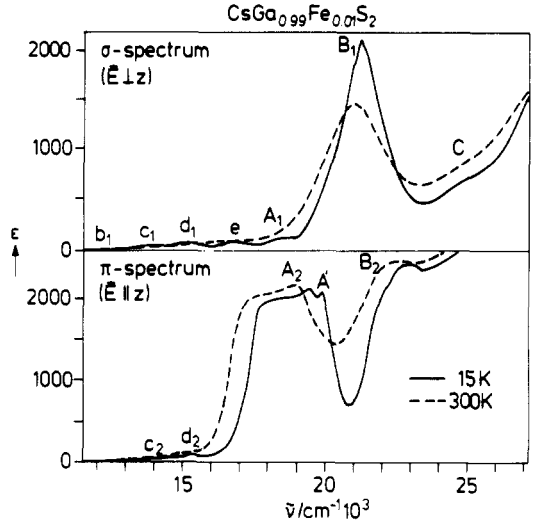


**Figure 2.** Polarized absorption spectra of a $CsGa_{0.99}Fe_{0.01}S_2$ single crystal (thickness $d = \sim 100\ \mu m$) recorded at room temperature (dashed lines) and at 15 K (solid lines) in different polarizations. Absorption intensities (given in L $mol^{-1}$ $cm^{-1}$) are approximate due to the difficulties of measuring the correct thicknesses.

**$Na_3FeS_3$.** The spectrum of the dark green salt is shown in a figure displayed in the supplementary material section. It is similar to $Na_5FeS_4$ but better resolved, the main bands A and B showing temperature dependent intensities.

Peaks at similar positions in common for the one- and two-center complex spectra supply arguments for CT transitions (cf. Table S1 in the Supplementary Material). The temperature dependence of the 19 200-$cm^{-1}$ band A′ is an indication for level doublings due to exchange-coupled metal ions.[35] The absorption spectrum of $[Fe_2S_2(S_2\text{-}o\text{-xyl})_2]^{2-}$, which also show higher intensities of CT bands at low temperature, have been interpreted as dimer excitations ($^6A_1{}^6A_1 \rightarrow {}^6A_1{}^6T_2$) as well.[45]

**$CsGa_{1-x}Fe_xS_2$ ($0.0 \le x \le 0.25$).** Crystal needles of $CsGa_{1-x}Fe_xS_2$ supply polarized spectra with the $\vec{E}$ vector of light perpendicular ($\sigma$-spectrum) or parallel ($\pi$-spectrum) to the optical axis ($z$ identical with the $[Ga(Fe)S_2]$ chain direction). The brown to black compounds have a metallic surface and appear yellow-green ($\vec{E} \perp z$) and deep-red ($\vec{E} \parallel z$) on a polarization microscope.

The host compound $CsGaS_2$ shows an absorption edge near 30 000 $cm^{-1}$ and some (predominantly $z$-polarized) weak bands between 18 400 and 25 500 $cm^{-1}$. In Figure 2 the polarized spectra of $CsGa_{0.99}Fe_{0.01}S_2$ are illustrated. The gaussian shaped band $B_1$ in the $\sigma$-spectrum is due to a CT transition because of its large extinction coefficient. At lower energy several weak absorptions ($\epsilon \sim 75$ L $mol^{-1}$ $cm^{-1}$) and a higher shoulder, C, can be detected.

In the $\pi$-spectrum a broad band, $A_2$, extending between 17 000 and 20 000 $cm^{-1}$ is shown which shifts at higher temperatures towards lower energies. This feature is characteristic for a band edge as has been observed in optical spectra of other one-dimensional compounds, e.g., Wolfram's red salt.[53] A sharp peak, A′, appears obviously at low temperature. The second strong band $B_2$ occurs only in the $\pi$-spectrum. Since it was impossible to prepare thinner items from the brittle crystals to avoid high extinctions the measurements are limited to 25 000 $cm^{-1}$ in $z$- and 27 000 $cm^{-1}$ in $x,y$-polarization. While mixed crystals with increasing iron concentration $x$ exhibit a similar $\sigma$-spectrum, the band edge A of the $\pi$-spectrum undergoes a substantial red shift, and the low-energy bands, e.g. $d_2$, gain intensity. Due to the metallic surface, measurements of higher-doped crystals were impossible.

For discussing low symmetry effects that point group will be used which supplies large contributions of d orbital splittings.

(41) Rivoal, J. C.; Briat, B. *Mol. Phys.* **1974**, *27*, 1081.
(42) Lane, R. W.; Ibers, J. A.; Frankel, R. B.; Papaefthymiou, G. C.; Holm, R. H. *J. Am. Chem. Soc.* **1977**, *99*, 84.
(43) Muraoka, T.; Nozawa, T.; Hatano, M. *Chem. Lett.* **1976**, 1373.
(44) Muraoka, T.; Nozawa, T.; Hatano, M. *Bioinorg. Chem.* **1978**, *8*, 45.
(45) Muraoka, T.; Nozawa, T.; Hatano, M. *Inorg. Chim. Acta* **1988**, *154*, 59.
(46) Millar, M.; Lee, J. F.; Koch, S. A.; Fikar, R. *Inorg. Chem.* **1982**, *21*, 4105.
(47) Ueyama, N.; Nakata, M.; Nakamura, A. *Bull. Chem. Soc. Jpn.* **1981**, *54*, 1727.
(48) Nakata, M.; Ueyama, N.; Terakawa, T.; Nakamura, A. *Bull. Chem. Soc. Jpn.* **1983**, *56*, 3647.
(49) Eaton, W. A.; Lovenberg, W. *J. Am. Chem. Soc.* **1970**, *92*, 7195.
(50) Ulmer, D. D.; Holmquist, B.; Vallee, B. L. *Biochem. Biophys. Res. Commun.* **1973**, *51*, 1054.
(51) Rivoal, J. C.; Briat, B.; Cammack, R.; Hall, D. O.; Rao, K. K.; Douglas, I. N.; Thomson, A. J. *Biochim. Biophys. Acta* **1977**, *493*, 122.
(52) Bennett, D. E.; Johnson, M. K. *Biochim. Biophys. Acta* **1987**, *911*, 71.
(53) Tanaka, M.; Kurita, S.; Kojima, T.; Yamada, Y. *Chem. Phys.* **1984**, *91*, 257.

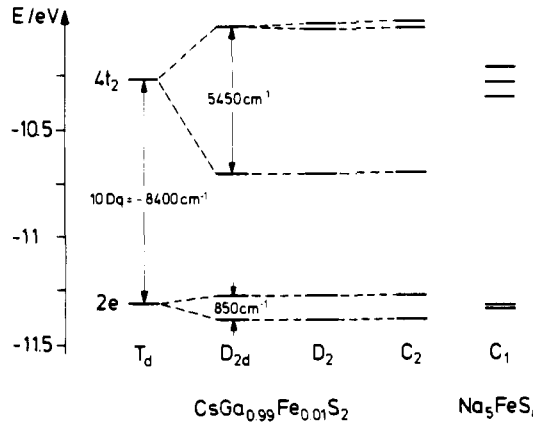


**Figure 3.** EHMO results of a $[Fe^{III}S_4]$ chromophore for higher symmetry ($T_d$, $D_{2d}$, $D_2$) and real ($C_2$ for $CsGa_{0.99}Fe_{0.01}S_2$,[10] $C_1$ for $Na_5FeS_4$[6]) coordination geometries (Fe–S distance in the former cases are set to 227.7 pm; EHMO parameters for Fe and S are adopted from Silvestre and Hoffmann,[34] with the Helmholtz–Wolfsberg constant $k = 1.75$). Only the d-orbitals of iron are illustrated.

**Table III.** Splitting of the Cubic Sextet LMCT Levels of a High-Spin $d^5$ Chromophore on Tetragonal Perturbation (Along the $S_4$ Axis of the Tetrahedron, $D_{2d}$ Symmetry)

| $T_d$ | $D_{2d}$ | polarization[a] |
|---|---|---|
| $^6A_1$ | $^6A_1$ | ground state |
| $^6T_2$ | $^6B_2$ | $z$ |
| | $^6E$ | $x, y$ |
| $^6T_1$ | $^6A_2$ | |
| | $^6E$ | $x, y$ |
| $^6E$ | $^6A_1$ | |
| | $^6B_1$ | |
| $^6A_2$ | $^6B_1$ | |

[a] In $D_{2d}$ symmetry the electric dipole operator transforms like $e(x,y)$ and $b_2(z)$.

Extended Hückel (EHMO) calculations performed for a $[FeS_4]$ tetrahedron distorted until the symmetry reaches the point group $C_2$, which is the site symmetry of gallium (or iron) in $CsGa_{0.99}Fe_{0.01}S_2$10, result in d-orbital splittings as illustrated in Figure 3. Obviously a $[FeS_4]$ tetrahedron distortion down to $D_{2d}$ exerts the largest effects on the orbital structure such that this symmetry should be the most useful group which still furnishes selection rules. An EHMO calculation on the $Na_5FeS_4$ (with crystal structure data of ref 6) is also given for comparison which would support the choice of cubic symmetry used for the isolated compound.

From magnetic data[10] a high-spin ground state is assumed for $CsGa_{0.99}Fe_{0.01}S_2$ as well as for $Na_5FeS_4$. Table III presents possible symmetries of LMCT levels (given in Table I) on $D_{2d}$ distortion and resulting polarizations of transitions. The $^6T_2$ states split into a $z$-polarized $^6B_2$ and a $x,y$-polarized $^6E$ component. Another $^6E$ results from the $^6T_1$ level; however, excitations from the $^6A_1$ ground state are expected to be of lower intensity since the corresponding cubic transitions to $^6T_1$ is symmetry forbidden. Hence, the intense $z$-polarized bands $A_2$ and $B_2$ in Figure 2 can be assigned to transitions $^6A_1(A_1) \rightarrow {}^6B_2(T_2)$ and the $x,y$-polarized band $B_1$ to $^6A_1(A_1) \rightarrow {}^6E_2(T_2)$ with $T_d$ symbols in brackets.

Comparison of LMCT bands to corresponding orbital transitions of the complex monomer can be made using Tables II and IV. From similar band positions in the spectra of $Na_5FeS_4$ and $CsGa_{0.99}Fe_{0.01}S_2$, one can conclude that the band $A_2$ in Figure 2 obviously belongs to the lowest orbital transition $1t_1 \rightarrow 2e$. Accordingly $B_2$ arises from $1t_1 \rightarrow 4t_2$, the energy interval of $A_2$ and $B_2$ corresponding to $10Dq$. The shoulder C in the $\sigma$-spectrum is paralleled by the weak absorption C of $Na_5FeS_4$ and is therefore due to an orbital transition $3t_2 \rightarrow 2e$. By deconvolution of the $x,y$-polarized room temperature spectrum of $CsGa_{0.99}Fe_{0.01}S_2$ into Gaussian components, another band D at 27 500 $cm^{-1}$ is identified, which is assigned to $3t_2 \rightarrow 4t_2$.

**Table IV.** Assignment of CT Bands in the Polarized Absorption Spectrum Measured from $CsGa_{0.99}Fe_{0.01}S_2$ Single Crystals

| energy, $cm^{-1}$ | | | orbital transition | | excited level | |
|---|---|---|---|---|---|---|
| 300 K | 15 K | polarizn | $T_d$ | $D_{2d}$ | $D_{2d}$[a] | peak |
| | 18 600 sh | $\sigma$ | $1t_1 \rightarrow 2e$ | $e \rightarrow ?$ | $^6E(T_2)$ | $A_1$ |
| 17 150– | 17 860 | | | | | |
| 19 160 | 18 320 | $\pi$ | $1t_1 \rightarrow 2e$ | $a_2 \rightarrow b_1$ | $^6B_2(T_2)$ | $A_2$ |
| | 19 410 | | | | | |
| | 19 910 | $\pi$ | | | | A′ |
| 21 000 | 21 340 | | | | | |
| | 22 100 sh | $\sigma$ | $1t_1 \rightarrow 4t_2$ | $e \rightarrow b_2$ | $^6E(T_2)$ | $B_1$ |
| 22 200 | 22 700 | $\pi$ | $1t_1 \rightarrow 4t_2$ | $e \rightarrow e$ | $^6B_2(T_2)$ | $B_2$ |
| 25 000 sh | 25 000 sh | $\sigma$[b] | $3t_2 \rightarrow 2e$ | ? | $^6E(T_2)$ | C |
| | 27 500 sh[c] | $\sigma$ | $3t_2 \rightarrow 4t_2$ | ? | $^6E(T_2)$ | D |

[a] Cubic parent state in parentheses. [b] The measurement of the $\sigma$-polarized spectrum is limited to 25 000 $cm^{-1}$. [c] From band analysis.

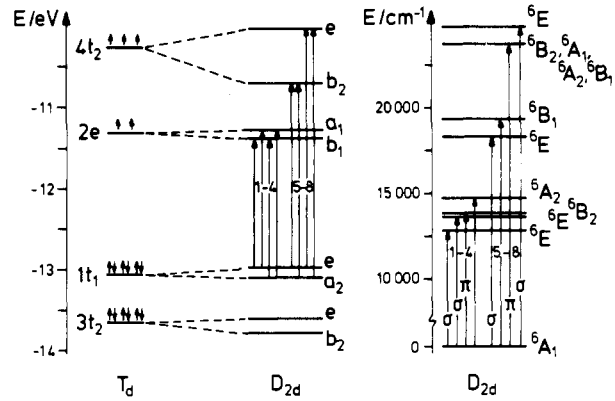


**Figure 4.** EHMO calculations for a $[Fe^{III}S_4]$ chromophore in $CsGa_{0.99}Fe_{0.01}S_2$ with $T_d$ and $D_{2d}$ symmetry ($\alpha = 99.20°$, Fe–S distance 227.7 pm) and electron occupation for a high-spin ground state. The transitions 1–8 corresponding to orbital differences are relevant for discussing the lowest LMCT bands. On the right, the energy level scheme of sextet LMCT states are given as they result from orbital energy differences (no explicit electron repulsion).

For more information about directions and low-symmetry splittings of cubic $^6T_2$ states, we consult EHMO results for tetragonal distorted ($MS_2$ angle 99.2°, $D_{2d}$) $[Fe^{III}S_4]$ chromophores (cf. Figure 4).

Obviously the only significant effect of $S_4$ distortion is on the cubic $4t_2$-MO due to $\sigma$-antibonding. The diagram on the right-hand side shows the corresponding energy level scheme, the splittings of which result from the orbital energy differences. The term symbols were determined from the symmetry of Heisenberg–Slater determinants constructed from the excited electron configurations in $D_{2d}$ symmetry (omitting doublet and quartet states). Except for orbital transition no. 7 only one sextet state results out of each excited electron configuration.

All LMCT levels resulting from the cubic orbital transition $1t_1 \rightarrow 2e$ (i.e. 1–4 in Figure 4) are calculated within 1000 $cm^{-1}$, one, $^6E$, being the lowest. It cannot be decided whether this $^6E$ arises from $^6T_2$ of $T_d$, since eigenfunctions of $^6T_1$ and $^6T_2$ LMCT levels are not available. An assignment of $B_1$ (Figure 2) to the lowest cubic orbital transition about 3000 $cm^{-1}$ (experiment) higher than $A_2$ would strongly disagree with EHMO calculations. Also no predictions can be made for the type of tetragonal splitting of $^6T_2$ from the second orbital transition $1t_1 \rightarrow 4t_2$, which again is a result of undistinguishable $^6E$ terms.

Informations about level orders of LMCT states may be obtained also from AOM calculations on $d^{N+1}$ metal orbital configuration applicable after completion of electron transfer.[54] This model considers electron–electron interaction on the iron center by Racah parameters B and C. With $B = 460$ $cm^{-1}$ and $C = 1800$ $cm^{-1}$ obtained from fitting d–d transitions of the $[FeS_4]$

(54) Vanquickenborne, L. G.; Verdonck, E. *Inorg. Chem.* **1976**, *15*, 454.

chromophore (see d–d section below) and $Dq_{tet} = -390$ cm$^{-1}$, calculations of a $d^6$ electron configuration were carried out for the cubic and for the tetragonally distorted tetrathioferrate chromophore (the latter based on corresponding AOM parameters). For obtaining level symmetries of excited LMCT states, the resulting $d^6$ multiplets are combined with those of the ligand orbital from which the electron transition originates (direct product of corresponding irreducible representation and vector addition of spin moments). Since only sextet LMCT states give rise to spin-allowed transitions (Table I), calculation of relative energies of $d^6$ quintet levels will suffice. For $^5E$ resulting from an electron transition into the 2e metal orbital, the low symmetry splitting $^5A_1$–$^5B_1$ is 200 cm$^{-1}$ for the higher $^5T_2$ state from transition into $4t_2$; the splitting $^5E$–$^5B_2$ is 1325 cm$^{-1}$. Although the energy differences obtained from the AOM are smaller than those from the preceding EHMO calculations (cf. Figure 4), the qualitative result is the same, and it is unlikely that the $B_1$ band in Figure 2 belongs to the lowest orbital transition ($1t_1 \rightarrow 2e$). The energy difference between the $D_{2d}$ levels resulting from $1t_1 \rightarrow 4t_2$, estimated as 1325 cm$^{-1}$ from the AOM, agrees with the experimental difference of $B_1$ and $B_2$ (cf. Table IV).

Symmetries of $D_{2d}$ LMCT levels are $^6B_1$, $^6E$ (for parent state $^5B_2$) and $^6A_1$, $^6A_2$, $^6B_1$, $^6B_2$, $^6E$ (for the parent $^5E$ of $1t_1 \rightarrow 4t_2$). Again a distinction between $^6E(T_2)$ and $^6E(T_1)$ cannot be made; however, due to the agreement between experiment and EHMO calculation on the degree of the $B_1$–$B_2$ band splitting, we have good reason to assign the intense peak $B_1$ to the CT excitation into $^6E$ resulting from the $^5B_2$ parent state which is symmetry and spin allowed.

In Table IV the assignments of CT bands in the $CsGa_{0.99}Fe_{0.01}S_2$ spectra resulting from the above discussions are listed. A critical point is the lack of an intense absorption in $x,y$-polarization arising from the LMCT transition $^6A_1(A_1) \rightarrow {}^6E(T_2)$ ($1t_1 \rightarrow 2e$). A candidate for this transition is the band $A_1$ with an intensity of about 100 L mol$^{-1}$ cm$^{-1}$ observed in the $\sigma$-spectrum. Low intensities of this order also have been claimed for the third symmetry and spin allowed cubic LMCT transition in the spectra of $[FeCl_4]^-$ [24] and presently of $Na_5FeS_4$ which only appear as a weak shoulder. Another way of explaining $A_1$ would be an assignment to a d–d transition (see LF calculations below). For a final decision further investigations are necessary.

The peak A′ detected in the 15 K $\pi$-spectrum of $CsGa_{0.99}Fe_{0.01}S_2$ exhibits the same temperature behavior as the corresponding feature in the $Na_3FeS_3$ spectrum which is an indication for a pair transition. This leads to the conclusion that significant antiferromagnetic coupling of iron centers occur already at low iron concentrations in the $CsGaS_2$ host. Also the band edge character of $A_2$ shows the operation of solid state effects on the $\pi$-spectrum. The bathochromic shift of $A_2$ observed for higher iron concentrations is explained by a growth of $[FeS_2]$ oligomers similar to shifts of the lowest $\pi \rightarrow \pi^*$ transitions in absorption spectra of conjugated organic polyenes with increasing lengths. In $x,y$-polarization the CT band $B_1$ has, on the other hand, a Gaussian profile independent on the degree of iron concentration.

Proposed band assignments compare well with those of isolated high-spin $[FeS_4]$ chromophores (see also d–d transitions). A change of ground state when increasing the iron concentration, which has been claimed because of the low magnetic moments, would give rise to an absorption curve of very different shape. In conclusion, the mixed crystal spectra (Figure 2) demonstrate an unusual anisotropy: The $\sigma$-spectra ($\vec{E} \perp z$) arise from levels localized on isolated $[FeS_4]$ units, while the $\pi$-spectra ($\vec{E} \parallel z$) indicate delocalized levels due to the extended electronic structure of LMCT levels.

**$AFeS_2$ (A = K, Rb, Cs).** A characteristic spectrum of $CsFeS_2$ in a KBr pellet is illustrated in Figure 5. Different alkali-metal cations do not cause significant changes of the absorption curve.[17,18] Temperature effects are noticed, e.g., in the low-energy band A changing its maximum in the 15K spectrum compared to room temperature. Unfortunately no polarized spectra could be recorded from these complexes due to the large metallic reflection of the surfaces.

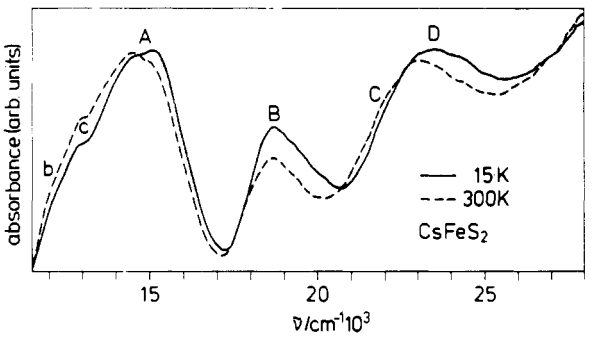


**Figure 5.** Absorption spectra of $CsFeS_2$ measured from a KBr disk at room temperature and at 15 K.

**Table V.** Assignment of CT Bands in the Absorption Spectrum of $AFeS_2$ (A = Cs, Rb, K)

| energy, cm$^{-1}$ | | | orbital | excited level | |
|---|---|---|---|---|---|
| $CsFeS_2$[a] | $RbFeS_2$[a] | $KFeS_2$[a] | transition[b] | (cubic) | peak |
| 14 600 sh | 14 000 sh | 14 600 sh | d–d? | | |
| 15 100 | 15 200 | 15 100 | $1t_1 \rightarrow 2e$ | $^6T_2$ | A |
| | | 18 000 sh | ? | | |
| 18 700 | 18 800 | 18 900 | $1t_1 \rightarrow 4t_2$ | $^6T_2$ | B |
| 19 400 sh | 19 700 sh | 19 400 sh | ? | | |
| 22 100 sh | 22 000 sh | 21 900 sh | $3t_2 \rightarrow 2e$ | $^6T_2$ | C |
| | | 22 800 sh | ? | | |
| 23 100 | 23 400 | 23 600 | $3t_2 \rightarrow 4t_2$ | $^6T_2$ | D |
| 24 100 sh | 24 900 sh | 24 500 sh | ? | | |

[a] Measured as KBr disks at 15 K. [b] Notation for a single $[Fe^{III}S_4]$ center.

Comparing the energies of the lowest high intensity transition in the series $Na_5FeS_4$ (17 500 cm$^{-1}$), $CsGa_{1-x}Fe_xS_2$ with $x = 0.01$ (17 200 cm$^{-1}$), $x = 0.05$ (16 000 cm$^{-1}$), and $x = 0.10$ (15 600 cm$^{-1}$), and $CsFeS_2$ (14 600 cm$^{-1}$), one can conclude that band A in Figure 5 must be charge-transfer in origin as well. This assignment is supported by absorption measurements of colloidal $[NaFeS_2]_x$ (also consisting of linear $[Fe^{III}S_2]$ chains), which supplies intensities of about 8000 L mol$^{-1}$ cm$^{-1}$ for the corresponding maximum.[55] Earlier measurements[18] yielding much lower intensities for $KFeS_2$ and $RbFeS_2$ are apparently incorrect.

The bathochromic shift of about 3000 cm$^{-1}$ of the lowest CT band A compared to $Na_5FeS_4$ is also observed for the band B and the shoulder C. Due to the otherwise close similarity of the absorption curves these bands are assigned to the corresponding cubic orbital transitions of the isolated $[FeS_4]$ chromophore (cf. Tables II and V). Similarly band D should belong to the next higher LMCT transition ($3t_2 \rightarrow 4t_2$).

**d–d Transitions. $CsGa_{1-x}Fe_xS_2$ ($0.01 \leq x \leq 0.25$).** The low temperature spectra of $CsGa_{1-x}Fe_xS_2$ recorded at high sensitivity show several well-resolved absorptions in the range between 8000 and 18500 cm$^{-1}$ which due to their low intensities ($\epsilon \leq 75$ L mol$^{-1}$ cm$^{-1}$ with respect to one Fe complex unit) should belong to d–d transitions. Figure 6 illustrates the long wavelength part, the pertinent intensities being very low ($\epsilon \leq 1$ L mol$^{-1}$ cm$^{-1}$). For small iron content (Figure 6a) this region could only be measured from concentrated KBr disks using our device used for scattering samples (ESS), from mixed crystals with higher iron concentrations ($x \geq 0.07$) also single crystal spectra were recorded (Figure 6b). Polarized spectra of $CsGa_{0.85}Fe_{0.15}S_2$ (Figure 6c) show, that all bands are predominantly $\sigma$-polarized while in the $\pi$-spectrum a large background absorbance does not allow to identify discrete bands. Well resolved spectra in the near-IR

(55) You, J. F.; Snyder, B. S.; Papaefthymiou, G. C.; Holm, R. H. *J. Am. Chem. Soc.* **1990**, *112*, 1067.

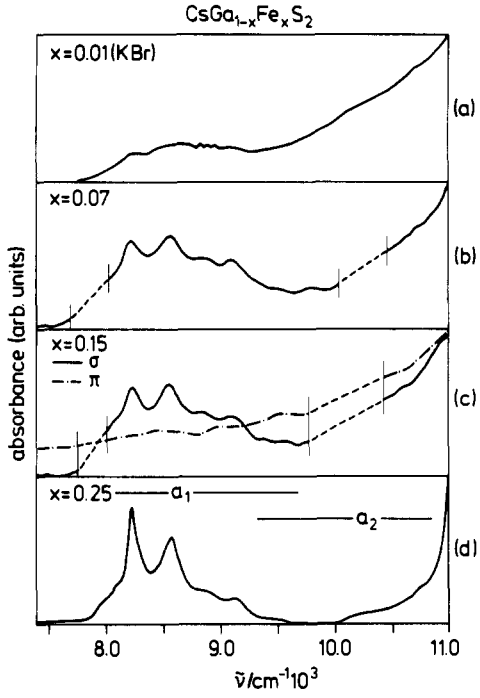


**Figure 6.** Near-IR absorption spectra of $CsGa_{1-x}Fe_xS_2$ measured with different techniques: (a) $CsGa_{0.99}Fe_{0.01}S_2$ from a highly doped KBr disk at 20 K on the ESS device; (b) $CsGa_{0.93}Fe_{0.07}S_2$ single crystal measured at 15 K on the Cary 17 instrument (the dashed regions are disturbed by atmospheric absorptions); (c) $CsGa_{0.85}Fe_{0.15}S_2$ single crystals at 15 K on the Cary 17 (polarized spectra); (d) $CsGa_{0.75}Fe_{0.25}S_2$ single crystal recorded at 20 K on ESS.

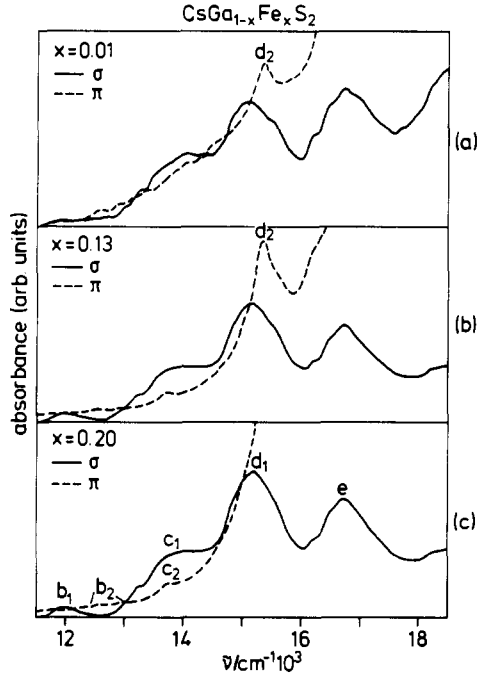


**Figure 7.** d–d spectral region in the polarized spectra of $CsGa_{1-x}Fe_xS_2$ with different iron contents measured at 15 K.

region were obtained from a $CsGa_{0.75}Fe_{0.25}S_2$ crystal by using again the ESS device for recording scattering samples (Figure 6d). With increasing iron content in the crystal the spectra obviously become better resolved.

This is also the case in the $\sigma$-spectrum toward higher energy shown in Figure 7a–c. The $\pi$-spectra are obscured toward higher energy due to the background absorption caused by the lowest LMCT band $A_2$ (cf. Figure 2). The $d_2$ peak obtains intensity with larger iron content and is covered by $A_2$ in the spectrum of the $x = 0.20$ compound. The increased intensity of $d_2$ is a manifestation of stolen intensity depending on the energy difference between $d_2$ and $A_2$ the latter undergoing a bathochromic shift for larger $x$ (see above).[31]

**Table VI.** Assignment of *Inter*configurational d–d Transitions in the Polarized Absorption Spectra of $CsGa_{1-x}Fe_xS_2$ ($0.01 < x < 0.25$) Mixed Crystals

| energy, cm$^{-1}$ | center of gravity, cm$^{-1}$ | polarization | excited level $D_{2d}$ | peak |
|---|---|---|---|---|
| 7 960 sh 8582<br>8 100 sh 8880<br>8 224 9134[a]<br>8 320 sh 9480[a]<br>8 440 sh 9580 sh[a] | 8 520[b] | $x, y$[c] | $^4E(T_1(G))$ | $a_1$ |
| 8 520 sh<br>10 210 sh<br>10 760 sh | ~10 500 | $x, y$[c] | $^4A_2(T_1(G))$ | $a_2$ |
| 11 430<br>11 980<br>12 300 sh<br>12 650 sh | 11 900 | $x, y$ | $^4E(T_2(G))$ | $b_1$ |
| 12 220 sh<br>12 620<br>13 070 | 12 700 | $z$ | $^4B_2(T_2(G))$ | $b_2$ |

[a] These bands may also arise from an excitation into the $^4A_2(T_1(G))$ level. [b] For the range between 7900 and 9600 cm$^{-1}$. [c] In addition some uncertain $z$-polarized peaks (Figure 6c).

The spectroscopic findings in the LF region also do not indicate any change of the ground state on iron content increase; no new bands appear in the spectra of the highly doped compounds. Therefore a high-spin energy scheme is appropriate for assigning the d–d transitions.

Following symmetry selection rules for the $D_{2d}$ point group given in Table III, we assign the longest $x,y$-polarized wavelength band feature $a_1$ (Figure 6) to the transition $^6A_1(A_1(S)) \rightarrow {}^4E(T_1(G))$ which is an interconfigurational excitation ($e^2t_2^3 \rightarrow e^3t_2^2$ in cubic notation). Due to increased $\sigma$-antibonding leading to larger equilibrium distances in the excited state, the spectrum in this region shows several well-resolved peaks which are attributed to vibronic transitions. An assignment to the $^4A_2$ component of $^4T_1(G)$ is more difficult, since transition into this is forbidden in $D_{2d}$ symmetry. The two weak shoulders $a_2$ at about 10 500 cm$^{-1}$ are good candidates for this. The $\sigma$ polarized band $b_1$ (Figure 7) is due to a transition into $^4E(T_2(G))$, and the two weak features $b_2$ in the $\pi$-spectrum are assigned to an excitation into $^4B_2(^4T_2(G))$. The proposed assignments to these low-energy levels are listed in Table VI.

Assignments of transitions within the $e^2t_2^3$ configuration follow the interpretation proposed for $[FeCl_4]^-$.[25] Accordingly, the bands $c_1$ and $c_2$ observed in either polarization belong to transition into $^4A_1$, $^4E(G)$ (cf. Table VII). AOM calculations (see below) indicate that splitting due to tetragonal distortion is relatively small. Therefore the features between 13 250 and 14 050 cm$^{-1}$ in the $\sigma$-spectrum are more likely due to vibrational sidebands. The $\sigma$ polarized peak $d_1$ is assigned to an excitation into the $^4E$ component of $T_2(D)$ while the sharp band $d_2$ observed in the $\pi$-spectra of mixed crystals with $x \leq 0.13$ arises from a transition into $^4B_2$ of the same $^4T_2(D)$. This assignment is supported by the shape of $d_1$ which is broader than for $d_2$. Inclusion of spin–orbit coupling ($\zeta = 370$ cm$^{-1}$)[56] in the AOM calculations supplies a larger splitting of $^4E$ than for $^4B_2$. Band e is attributed to a transition into low-symmetry components of cubic $^4E(D)$. Although these transitions are forbidden, the intensity of e is observed having the same order as $d_1$, as is the case in the corresponding transition of $[FeCl_4]^-$.[25] The reason might be due to the neighborhood of CT bands supplying intensity by vibronic coupling mechanisms. The nature of the $\sigma$-polarized band $A_1$ (see Table

(56) Ewald, A. H.; Martin, R. L.; Sinn, E.; White, A. H. *Inorg. Chem.* **1969**, *8*, 1837.

**Table VII.** Assignment of *Intra*configurational d–d Transitions in the Polarized Absorption Spectra of $CsGa_{1-x}Fe_xS_2$ ($0.01 < x < 0.25$) Mixed Crystals

| energy, $cm^{-1}$ | center of gravity, $cm^{-1}$ | polarizn | excited level $D_{2d}$ | peak |
|---|---|---|---|---|
| 13 250<br>13 560<br>13 670 sh<br>13 850 sh<br>14 050 | 13 600 | $x, y$ | $^4A_1(A_1(G))$<br>$^4A_1(E(G))$<br>$^4B_1(E(G))$ | $c_1$ |
| 13 600 | 13 600 | $z$ | $^4A_1(A_1(G))$<br>$^4A_1(E(G))$<br>$^4B_1(E(G))$ | $c_2$ |
| 14 620 sh<br>14 870 sh<br>15 160<br>15 300 sh<br>15 540 sh<br>15 840 sh | 15 170 | $x, y$ | $^4E(T_2(D))$ | $d_1$ |
| 14 390 sh<br>15 000 sh<br>15 360<br>15 610 sh | 15 300 | $z$ | $^4B_2(T_2(D))$ | $d_2$ |
| 16 180 sh<br>16 460 sh<br>16 680<br>16 850 sh<br>17 480 sh | 16 800 | $x, y^a$ | $^4A_1(E(D))$<br>$^4B_1(E(D))$ | e |
| 18 210 sh<br>18 450<br>18 690 sh<br>19 100 sh | 18 600 | $x, y$ | $^4A_2(T_1(P))$ or LMCT | $A_1$ |

[a] $z$-polarized d–d spectrum is dominated by LMCT bands (Figure 2).

VII) with lower intensity than e cannot be clarified on the present basis. It may arise from a (symmetry-forbidden) d–d transition (e.g., into $^4A_2(T_1(P))$) or from the lowest LMCT excitation (see previous section).

Support for the assignments given in Tables VI and VII is given by AOM calculations. Unfortunately the level energies of pseudotetrahedral high-spin $d^5$ systems depend only very weakly on the AOM parameter $e_\pi$. This is not unique for $d^5$ but is also the case for the tetrahedral $d^7$ configuration as discussed for $[CoCl_4]^{2-}$ [28] and $[CoS_4]^{6-}$.[37] Therefore an evaluation of $e_\pi$ from the spectrum is not possible. Since the independence of d–d transitions on $e_\pi$ also extends to very small parameter values, we can set $e_\pi = 0$ in our calculations. The remaining three parameters $10Dq \equiv -(4/3)e_\sigma$, $B$, and $C$ are then determined by a total of eight experimental data. This allows the covariation of the $MS_2$ angle $\alpha$ which describes the degree of tetragonal distortion $S_4$ in the molecular chain. The starting value for $\alpha$ was set to 99.2° in accordance with the crystal structure data for $CsGa_{0.99}Fe_{0.01}S_2$, which is close to those for $CsGaS_2$.[57] The best fit to the experimental energies was achieved by using the parameters $e_\sigma$ = 4260 $cm^{-1}$ ($Dq$ = −568 $cm^{-1}$), $B$ = 460 $cm^{-1}$, $C$ = 1800 $cm^{-1}$ and $\alpha$ = 102.4° (cf. Table VIII). This $\alpha$ angle is between the experimental value of $CsGaS_2$ and that of the pure ferric chain of $AFeS_2$ (~105° [15]). This local distortion is an indication of the presence of $FeS_2$ clusters in the $Ga(Fe)S_2$ chain.

Deviations of calculated energies from experimental data mainly concern the interconfigurational transitions. A reason for this may be the larger splittings of these bands due to vibrational fine structure which makes an estimation of gravity centers difficult. Calculations for nuclear configurations with real symmetry $C_2$ estimate the tetragonal $^4E$ level splittings lower than 100 $cm^{-1}$. Energy changes resulting from different Fe–S distances in the mixed crystals[10] are also negligibly small when a $R^{-5}$ dependence of $e_\sigma$ is assumed.

(57) Unpublished structure data.

**Table VIII.** AOM Calculation for the Tetragonally Distorted $[Fe^{III}S_4]$ Chromophore in $CsGa_{1-x}Fe_xS_2$ ($e_\sigma$ = 4260 $cm^{-1}$, $e_\pi$ = 0, $B$ = 460 $cm^{-1}$, $C$ = 1800 $cm^{-1}$, $\alpha$ = 102.4°) Neglecting Spin–Orbit Coupling

| transition | | energy, $cm^{-1}$ | |
|---|---|---|---|
| $T_d$ | $D_{2d}$ | calc | exp[a] |
| $^6A_1(S) \rightarrow {}^4T_1(G)$ | $^6A_1 \rightarrow {}^4E$ | 8 910 | 8 520 |
| | $\rightarrow {}^4A_2$ | 10 125 | 10 500 |
| $\rightarrow {}^4T_2(G)$ | $\rightarrow {}^4E$ | 11 429 | 11 900 |
| | $\rightarrow {}^4B_2$ | 12 415 | 12 700 |
| $\rightarrow {}^4A_1, {}^4E(G)$ | $\rightarrow {}^4B_1$ | 13 599 | 13 600 |
| | $\rightarrow 2{}^4A_1$ | 13 600 | |
| $\rightarrow {}^4T_2(D)$ | $\rightarrow {}^4E$ | 15 201 | 15 170 |
| | $\rightarrow {}^4B_2$ | 15 746 | 15 300 |
| $\rightarrow {}^4E(D)$ | $\rightarrow {}^4B_1$ | 16 818 | 16 800 |
| | $\rightarrow {}^4A_1$ | 16 820 | |
| $\rightarrow {}^4T_1(P)$ | $\rightarrow {}^4A_2$ | 18 691 | 18 600? |
| | $\rightarrow {}^4E$ | 19 618 | |

[a] Centers of gravity from Tables VI and VII.

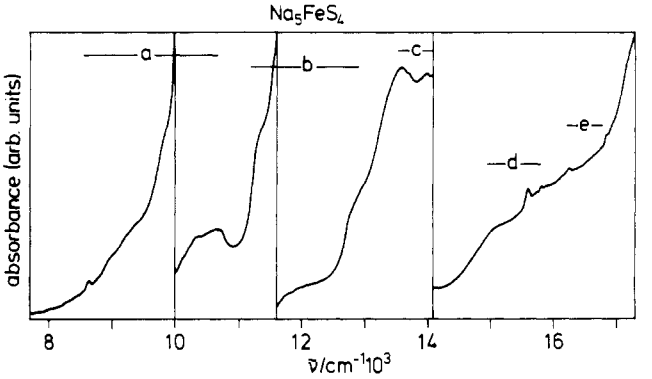


**Figure 8.** d–d absorption spectrum of $Na_5FeS_4$ measured from a KBr disk at 20 K on the ESS.

**Table IX.** Assignment of d–d Bands in the Absorption Spectrum of $Na_5FeS_4$ (KBr Disk at 20 K) and AOM Calculation[a]

| exp energy, $cm^{-1}$ | | center of gravity, $cm^{-1}$ | AOM calc, $cm^{-1}$ | excited level $T_d$ | peak |
|---|---|---|---|---|---|
| 8 630 | 9 750 | | | | |
| 8 940 | 10 250 | 9 000[b] | 9 053 | $^4T_1(G)$ | a |
| 9 400 | 10 650 | | | | |
| 11 250 | 11 900 | | | | |
| 11 600 | 12 800 | 11 700[b] | 11 607 | $^4T_2(G)$ | b |
| 13 600 | 14 000 | 13 600[b] | 13 600 | $^4A_1, {}^4E(G)$ | c |
| 15 150 | 15 820 | | | | |
| 15 600 | | 15 500[b] | 15 508 | $^4T_2(D)$ | d |
| 16 240 | 16 830 | c | 16 820 | $^4E(D)$ | e |
| 19 100 | | c | 19 343 | $^4T_1(P)$ | A′ |

[a] From $e_\sigma$ = 4390 $cm^{-1}$ ($Dq$ = −585 $cm^{-1}$), $B$ = 460 $cm^{-1}$, $C$ = 1800 $cm^{-1}$. [b] After subtraction of a linear background. [c] Partially superimposed by LMCT bands (Figure 1).

**$Na_5FeS_4$.** Ligand field absorptions of $Na_5FeS_4$ were observed in the wavelength region in Figure 8. Due to the limited quality of spectra recorded from KBr disks, the bands appear only as shoulders on an increasing background resulting from higher LMCT transitions. In particular in the region between 8600 and about 13 000 $cm^{-1}$, where the lowest interconfigurational transitions into $^4T_1(G)$ and $^4T_2(G)$ are expected, band locations in the spectrum are uncertain. In Table IX an assignment is presented which uses corresponding interpretations for $CsGa_{1-x}Fe_xS_2$. Accordingly, band c in Figures 1 and 8 is assigned to the intraconfigurational transition $^6A_1(S) \rightarrow {}^4A_1, {}^4E(G)$, d to transition into $^4T_2(D)$ and e into $^4E(D)$.

Fitting the band centers to parameters of a cubic AOM calculation leads to $e_\sigma$ = 4390 $cm^{-1}$ ($Dq$ = −585 $cm^{-1}$), $B$ = 460 $cm^{-1}$, and $C$ = 1800 $cm^{-1}$. This set is equal to that for the mixed crystals, only $e_\sigma$ is somewhat larger for $Na_5FeS_4$ which is, however, uncertain, since $e_\sigma$ primarily depends on the energies of the

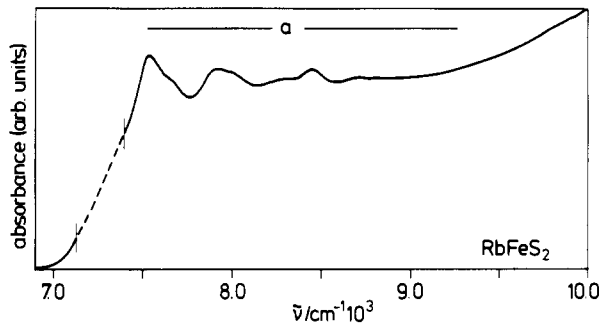


**Figure 9.** Near-IR absorption spectrum of $RbFeS_2$ recorded from a KBr disk at 20 K on the ESS. The dashed region is uncertain due to atmospheric absorptions.

**Table X.** Assignment of d–d Bands in the Absorption Spectra of $AFeS_2$ (KBr Disk at 15 or 20 K)

| energy, cm$^{-1}$ | | | | |
|---|---|---|---|---|
| $RbFeS_2$ | $KFeS_2$ | $CsFeS_2$[a] | excited level $T_d$ | peak |
| 7545 | ~7400[b] | ~7400[b] | | |
| 7650 sh | 7530 sh | 7590 sh | | |
| 7925 | 7780 | 7780 | | |
| 8020 sh | 7900 sh | | | |
| 8300 | 8160 | | $^4T_1(G)$ | a |
| 8450 | 8270 sh | | | |
| 8740 | | | | |
| 8930 | | | | |
| 12300 sh | 12200 sh | 12300 | | |
| 13000 sh | 12800 sh | 12700 sh | $^4T_2(G)$ | b |
| 14600 sh | 14000 sh | 14600 sh | $^4A_1$, $^4E(G)$? | c |

[a] Uncertain due to stray light effects. [b] Determination of band energy afflicted by atmospheric absorptions.

interconfigurational bands from which gravity centers are difficult to estimate. The theoretical results compiled in Table IX also furnish a possible assignment of A′ being due to a cubic LF transition into $^4T_1(P)$.

**$Na_3FeS_3$.** This compound is different from $Na_5FeS_4$, as bands below 11 000 cm$^{-1}$ are not detected; they may, however, be hidden under a steeply rising background. The features appearing in the 15 K spectrum between 12 800 and 16 100 cm$^{-1}$ (see the supplementary material) can be correlated to the same absorptions observed in the one-center complex spectrum. Therefore corresponding bands b, c, d, and e in the $Na_3FeS_3$ spectrum are assigned to d–d transitions of the isolated $[Fe^{III}S_4]$ chromophore as presented in Table IX. The antiferromagnetic coupling of high-spin iron centers is only manifested in the larger intensity of d. A ground state of lower multiplicity can be excluded.

**$AFeS_2$ (A = K, Rb, Cs).** Low-energy bands in the spectra of the chain compounds were measured from about 7400 cm$^{-1}$ on depending on the alkali-metal cation. Absorptions due to the atmosphere interfere with the spectra between 7100 and 7450 cm$^{-1}$. Therefore a complete spectrum could be taken only from the rubidium salt (Figure 9), while corresponding $KFeS_2$ and $CsFeS_2$ bands fall into the obscured region (Table X). The spectral fine structure followed by the first peak is similar to that of the mixed crystals $CsGa_{1-x}Fe_xS_2$ (cf. Figure 6) but has a bathochromic shift of about 700 cm$^{-1}$.

From the d–d absorption profiles in the near-IR region which are similar for all presently compounds investigated (cf. Figures 6, 8, and 9), we can conclude that the iron chromophores have high-spin $d^5$ character also in the chain compounds. The low magnetic moments reported[10,11,15] must then arise from strong antiferromagnetic coupling. In comparison, the lowest absorptions in Figure 9 can be assigned to the transition into cubic $^4T_1(G)$ of a $[Fe^{III}S_4]$ unit (which may be split by low-symmetry effects) and its vibrational fine structure. The bathochromic shift of these bands can be explained by shorter Fe–S distances (~223.0 pm) in the pure ferric chain compounds compared to the mixed crystals (~227.7 pm) due to the $Dq$ bond length dependence ($Dq \sim R^{-5}$) of the $^4T_1(G)$ level energy.[58] The higher d–d transitions are indicated by shoulders b and c (Table X) superimposed on the lowest LMCT band (Table V). The assignment of b to $^4T_2(G)$ and c to the lowest intraconfigurational transition into $^4A_1$, $^4E(G)$ must be, however, considered with caution. But from the near-IR spectrum (Figure 9), it is obvious that the high-spin ground state must be preserved, since from the theoretical energy formulas it is unlikely that the lowest transition $^2T_2 \rightarrow {}^4T_1$ of a hypothetical low-spin $d^5$ chromophore[18] could accidentally have an energy similar to the corresponding excitation in the high-spin system.

**Table XI.** AOM Calculation for the Tetragonally Distorted $[FeCl_4]^-$ Chromophore in $(PPh_4)[FeCl_4]$ ($e_\sigma$ = 4913 cm$^{-1}$, $e_\pi$ = 0, B = 444 cm$^{-1}$, C = 2728 cm$^{-1}$, $\alpha$ = 114.6°)

| LF transition | | energy, cm$^{-1}$ | |
|---|---|---|---|
| $T_d$ | $D_{2d}$ | calc | exp[25] |
| $^6A_1(S) \rightarrow {}^4T_1(G)$ | $^6A_1 \rightarrow {}^4A_2$ | 12 770 | 12 890 |
| | $\rightarrow {}^4E$ | 14 021 | 14 240 |
| $\rightarrow {}^4T_2(G)$ | $\rightarrow {}^4B_2$ | 15 326 | 15 210 |
| | $\rightarrow {}^4E$ | 16 184 | 16 050 |
| $\rightarrow {}^4A_1$, $^4E(G)$ | $\rightarrow {}^4B_1$ | 18 082 | 18 200 |
| | $\rightarrow 2{}^4A_1$ | 18 082 | |
| $\rightarrow {}^4T_2(D)$ | $\rightarrow {}^4E$ | 19 782 | 18 800 |
| | $\rightarrow {}^4B_2$ | 19 817 | |
| $\rightarrow {}^4E(D)$ | $\rightarrow {}^4B_1$ | 21 190 | 22 008 |
| | $\rightarrow {}^4A_1$ | 21 190 | |

## Discussion

**Nature of the Sulfur Ligand.** The present work demonstrates the close relationships of LF and CT spectra between a $[Fe^{III}S_4]$ chromophore and the corresponding tetrachloroferrate(III). This leads to the conclusion that the sulfur ligand in ternary iron(III) complexes behaves like common ligands (e.g., Cl, Br, $NH_3$, etc.) regarding its magnetical and optical behavior. This is also the case for crystalline $Na_6CoS_4$ containing isolated $[Co^{II}S_4]$ units which we have investigated for comparison.[37] The well-resolved d–d spectrum of this complex is also quite similar to that of the well-known $[CoCl_4]^{2-}$.[59-62]

To classify the sulfur ligand into the spectrochemical and nephelauxetic series we compare the AOM parameter sets of $[FeS_4]^{5-}$ and $[FeCl_4]^-$ at their actual symmetries. The latter complex has not been reported before. Therefore an AOM calculation in $D_{2d}$ symmetry was carried out using the crystal structure data of $(PPh_4)[FeCl_4]$ ($\alpha$ = 114.6° [25]) starting from the calculations on cubic symmetry.[25] A value of 4913 cm$^{-1}$ for $e_\sigma$ was obtained from $Dq$ = –655 cm$^{-1}$, where $e_\pi$ is set to zero because of the small dependence of transition energy on this parameter (see above). The results listed in Table XI reproduce the experimental data and low-symmetry splittings[25] quite well, although no fitting of parameters for this particular nuclear configuration was necessary. This again confirms the advantage of AOM parameters for low-symmetry fields since they are independent of the valence angles.

The parameters for the tetrachloro- and the tetrathioferrates(III) are listed in Table XII together with those of the cobalt(II) analogues. In either case the LF strength is lower for the sulfur than for the chlorine compounds which is in variance to what would be concluded from the spectrochemical series.[32] The smaller electron repulsion parameter $C$ in the thiocomplexes (for

(58) Marfunin, A. S. *Physics of Minerals and Inorganic Materials*; Springer-Verlag: Berlin, 1979.
(59) Cotton, F. A.; Goodgame, D. M. L.; Goodgame, M. *J. Am. Chem. Soc.* **1961**, *83*, 4690.
(60) Ferguson, J. *J. Chem. Phys.* **1963**, *39*, 116.
(61) van Stapele, R. P.; Beljers, H. G.; Bongers, P. F.; Zijlstra, H. *J. Chem. Phys.* **1966**, *44*, 3719.
(62) Jesson, J. P. *J. Chem. Phys.* **1968**, *48*, 161.

**Table XII.** Comparison of AOM Parameters ($cm^{-1}$) for Tetrathio and Tetrachloro Complexes of Iron(III) and Cobalt(II) ($e_\pi = 0$)

| | $[FeS_4]^{5-}$ | $[FeCl_4]^-$ | $[CoS_4]^{6-}$ [37] | $[CoCl_4]^{2-}$ [28] |
|---|---|---|---|---|
| $e_\sigma$ | 4390 | 4913 | 2160 | 2300 |
| $B$ | 460 | 444 | 600 | 740 |
| $C$ | 1800 | 2728 | 2600 | ?[a] |

[a] No data reported.

iron) and B (for cobalt) agrees with the common nephelauxetic series[32] and supports the trends of the covalent character.

For the optical electronegativity[31] of sulfur estimated from

$$\nu_{CT}(1t_1 \rightarrow 2e) = 30000[x_{opt}(\text{ligand}) - x_{opt}(\text{metal})] + \frac{8}{3}D$$

where $D$ is the spin-pairing energy,[63]

$$D = \frac{7}{6}\left(\frac{5}{2}B + C\right)$$

with Racah parameters $B = 460\ cm^{-1}$, $C = 1800\ cm^{-1}$, $x_{opt}(Fe^{3+}) = 2.5$,[64] and $\nu_{CT} = 18\,000\ cm^{-1}$ (for $Na_5FeS_4$, Table II), a value of $x_{opt}(S^{2-}) = 2.5$ is obtained. Previous work on other sulfur-coordinating ligands reports parameters in the range 2.4–2.95.[31,64]

**Influence of Antiferromagnetic Coupling on Optical Properties. CT Transitions.** The effect of antiferromagnetic coupling between iron centers by direct or indirect (superexchange involving ligand orbitals[65]) interactions on the CT spectra can be summarized as follows. (1) $Na_5FeS_4$ exhibits the usual LMCT spectrum of a tetrahedral high-spin $d^5$ chromophore in agreement with the respective magnetic Curie–Weiss behavior at temperatures higher than 28 K.[6] (2) The interaction of two iron centers in $Na_3FeS_3$ gives rise to some temperature dependent band intensities, but peak positions are nearly identical to those of the one-center complex. (3) The $\sigma$-spectra ($\vec{E} \perp$ chain axis) of mixed crystals can be explained from isolated tetrathioferrate(III) centers when tetragonal distortion is taken into account. (4) The $\pi$-spectra ($\vec{E} \parallel$ chain axis) of mixed crystals show for LMCT bands characteristic features of a band edge shifting to lower energies with increasing iron concentration. This is characteristic for electronic level delocalizations along the $[Ga(Fe)S_2]$ chain with higher iron content. (5) In the spectra of the pure ferric chain compounds $AFeS_2$, the LMCT bands exhibit a bathochromic shift of about 3000 $cm^{-1}$ compared to $Na_5FeS_4$, which does not interfere with an interpretation on the basis of isolated $[FeS_4]$ chromophores. This would justify calculations on isolated species also by more elaborate methods for explaining physical properties of $KFeS_2$.[24]

For a better orbital description of the ferric chain compounds $AFeS_2$ we calculated level dispersions by the extended-Hückel model. The results of these calculations are illustrated in Figure 10 showing the orbital energies for an isolated $[Fe^{III}S_4]$ chromophore at a mean Fe–S distance of 227.7 pm (from crystalline data of $CsGa_{0.99}Fe_{0.01}S_2$[57]) and results for a one-dimensional $[FeS_2]^-$ chain calculated from a band model. In either case a coordination of an exact tetrahedron at the iron center was presumed. Except for the Fe–S distance of 223.0 pm (from $CsFeS_2$[3]) the latter calculation is identical to that of Silvestre and Hoffmann.[34]

From the orbital scheme the lowest LMCT transition ($1t_1 \rightarrow 2e$) is calculated for the isolated $[FeS_4]$ chromophore to be at 14 171 $cm^{-1}$. Regarding the $[FeS_2]$ chain the occupations of band orbitals as proposed by Silvestre and Hoffmann can explain the reported semiconducting properties of $AFeS_2$,[15] where levels are fully occupied up to band 6 while bands 4–6 are only singly occupied, which is claimed to be favorable due to on-site electron

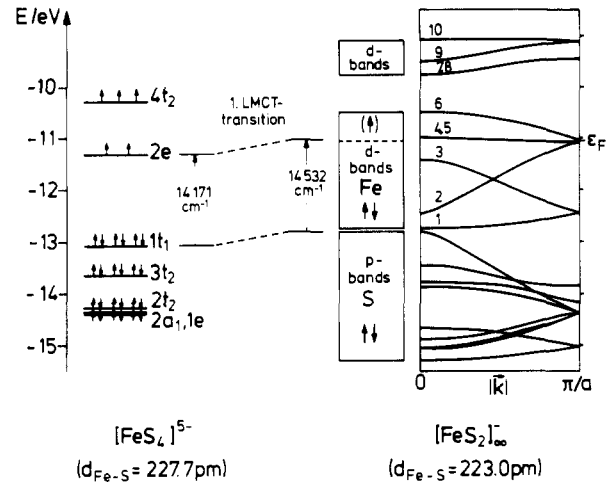


**Figure 10.** EHMO calculations of an isolated $[Fe^{III}S_4]$ chromophore and of an extended $[Fe^{III}S_2]$ chain obtained from a band model. The block diagram gives the electron occupations proposed by Sylvestre and Hoffmann.[34] The lowest LMCT energy results from the difference between the MOs $1t_1$ and 2e for the isolated unit; the energy gap between the highest ligand p band and the degenerate d band at $\vec{k} = 0$ is the corresponding energy for the chain.

repulsions.[34] According to the selection rule $\Delta\vec{k} = 0$ for the wave vector at respective maxima of level densities, the lowest LMCT will occur from the top of the highest ligand p-band to the top of the degenerate band 4,5 at $\vec{k} = 0$. The corresponding energy difference is calculated 14 532 $cm^{-1}$ which is larger than for the isolated $[FeS_4]$ center.

Extended-Hückel theory therefore cannot explain the bathochromic shift of the lowest CT band which is mainly due to neglect of explicit electron repulsion terms in this model. From the spin-pairing formula above we obtain a change of electron repulsion for the lowest LMCT transition ($1t_1 \rightarrow 2e$) of about 9000 $cm^{-1}$ with the Racah parameter values indicated. This value applying for delocalized electrons in a CT transition will be too large. However, the theoretical LMCT transitions calculated from orbital differences disagree with the experimental energies by more than 3000 $cm^{-1}$ for $Na_5FeS_4$ and mixed crystals of low iron content (Tables II and IV, while this discrepancy is only on the order of several hundred wavenumbers for $AFeS_2$ (Table V). The one-electron model obviously describes the energies of CT transitions (or corresponding band edges) of our extended $[Fe^{III}S_2]$ system much better. For the isolated $[Fe^{III}S_4]$ chromophore, on the other hand, a prediction of LMCT band energies by EHMO is inadequate due to the important role of electron repulsion in discrete molecules. Apparently the observed bathochromic shift is predominantly caused by a reduction of electron repulsion in the pure ferric chain compound compared to $Na_5FeS_4$ and $CsGa_{0.99}Fe_{0.01}S_2$.

**d–d Transitions.** Antiferromagnetic coupling obviously does not lead to a breakdown of LF interpretations of long wavelength absorptions. For all presently investigated compounds a high-spin ground state is maintained. Small variations of band energies are due to different coordination geometries and/or changes of the Fe–S distances in the chromophore. Intensity changes observed in the spectra of $Na_3FeS_3$ and $CsGa_{1-x}Fe_xS_2$ are caused by metal ion pair interactions or vibronic coupling to CT levels.

The d–d transition energies can be explained by common AOM calculations even when strong antiferromagnetic coupling between the iron centers is present. Unfortunately the intraconfigurational LF transitions of $AFeS_2$, whose excitation energies mainly depend on the electron–electron interaction, are superimposed by intense LMCT absorptions. Therefore, the reduction expected for this repulsion compared to $Na_5FeS_4$ (see previous section) cannot be confirmed from d–d spectra. Regarding the Racah parameters, it must be emphasized that all values obtained for the $[Fe^{III}S_4]$

(63) Jørgensen, C. K. *Orbitals in Atoms and Molecules*; Academic Press: London, 1962.
(64) Schmidtke, H.-H. *Ber. Bunsen-Ges. Phys. Chem.* **1967**, *71*, 1138.
(65) Jäger, E.; Perthel, R. *Magnetische Eigenschaften von Festkörpern*; Akademie Verlag: Berlin, 1983.

chromophores in our investigations are in the usual range of other compounds. The extreme parameters reported for $(NEt_4)[Fe(SR)_4]$ ($R = 2,3,5,6\text{-}(Me)_4C_6H$) ($B = 22\ cm^{-1}$, $C = 2222\ cm^{-1}$ [21,24]) apply for thiolates which absorb at lower energy. They might be explained by a breakdown of LF theory due to the large mesomeric electron system extending over the aromatic ligands. Also electron correlation which has been considered using unrestricted SW-X$\alpha$ calculations[25] could be a reason for this. Inverted bonding effects[25] where bonding MOs have more metal character than corresponding antibonding orbitals would not interfere with AOM results since the angular parts do not depend on d-electron delocalizations.

**Acknowledgment.** The authors are grateful to Prof. W. Bronger and Dr. P. Müller, who initiated the present work and supplied us with all compounds investigated. Also we are grateful to R. Linder for his helpful assistance carrying out the optical measurements and to K. Eifert and H. Adamsky for revising some of the computer programs.

**Supplementary Material Available:** A table of temperature dependent spectral data and assignments for $Na_3FeS_3$ and a figure showing the absorption spectrum of $NaFeS_3$ (2 pages). Ordering information is given on any current masthead page.